Open access • Journal Article • DOI:10.1039/C4NR04315D

300 mm Wafer-level, ultra-dense arrays of Au-capped nanopillars with sub-10 nm gaps as reliable SERS substrates — Source link

Jiaqi Li, Chang Chen, Hilde Jans, XiuMei Xu ...+7 more authors

Institutions: Katholieke Universiteit Leuven, Panasonic

Published on: 10 Oct 2014 - Nanoscale (The Royal Society of Chemistry)

Topics: Nanopillar, Immersion lithography and Wafer

Nanoscale

COMMUNICATION

View Article Online
View Journal | View Issue

Cite this: *Nanoscale*, 2014, **6**, 12391

Received 29th July 2014,
Accepted 27th August 2014

DOI: 10.1039/c4nr04315d

www.rsc.org/nanoscale

300 mm Wafer-level, ultra-dense arrays of Au-capped nanopillars with sub-10 nm gaps as reliable SERS substrates†

Jiaqi Li,*[a,b] Chang Chen,*[a,b] Hilde Jans,[a] Xiumei Xu,[a] Niels Verellen,[a,b] Ingrid Vos,[a] Yasuaki Okumura,[a,c] Victor V. Moshchalkov,[b] Liesbet Lagae[a,b] and Pol Van Dorpe[a,b]

The 193 nm deep UV immersion lithography is leveraged to fabricate highly dense and uniform arrays of Au-capped Si nanopillars on a 300 mm wafer level, and the substrates are applied in surface enhanced Raman spectroscopy for reliable molecule detection. Due to the sub-10 nm gap sizes and ultra-high array density with the lattice constant less than 100 nm, our nanopillar based substrates outperform the current commercial products in terms of the signal intensity, reproducibility and fabrication scale.

Introduction

Surface enhanced Raman spectroscopy (SERS) is a well-known and powerful molecular detection technique which is mainly enabled by the electromagnetic (EM) field enhancement on plasmonic nanostructured surfaces to compensate for the weak scattering cross sections of the target molecules. Extensive research has been carried out in the exploration of SERS substrates with enhanced and uniform signal generation. To obtain largely enhanced SERS intensities, regions of strongly enhanced EM field, referred to as plasmonic hot spots, are carefully engineered. This can be achieved by either adjusting the compositions and geometries of the nanostructures for a better aligned plasmonic resonance with the excitation and Raman scattering wavelengths,[1–3] or concentrating target molecules in gap-dominated small volumes.[4–6] Next to the SERS intensity, the uniformity of the SERS signal across the substrate and the reproducibility among different samples are extremely important. Plasmonic nanostructures formed by the self-assembly process can form regular arrays up to the millimeter scale with well controllable spacing and produce excellent signal uniformity.[7–10] The commercially available SERS substrate, Klarite™, consisting of gold layer coated arrays of inverted pyramids etched in silicon, highlights a reproducibility landmark with a better than 10% relative standard deviation level.[11,12] Although the reproducibility offered by the Klarite™ substrates is already a big improvement compared to aggregate-type substrates,[7] several applications require even better reproducibility and uniformity. In addition, the increase in reproducibility is typically accompanied by a drop in the SERS enhancement factor. Wafer-scale fabrication of uniform, reproducible and stable SERS substrates with a high enhancement factor remains a very critical step in the realization of commercial SERS applications.[13–16]

Nanopillar structures are one of the most promising SERS substrates in the sense that they provide a three-dimensional environment beneficial for molecular accessibility and formation of gap-rich plasmonic nanostructures.[14,15,17] Such substrates have been fabricated by a variety of techniques based on nanoimprint,[14] reactive ion etching,[15,17–19] chemical etching,[20,21] e-beam[17,22,23] and interference lithography,[24,25] as well as by anodic aluminum oxide templates.[3,5] Nevertheless, a high density of regularly spaced pillar substrates which is required for good signal reproducibility is still not achievable with most large scale lithography methods. Here we report a SERS substrate that is scalable and inherently uniform with a large enhancement factor. As schematically described in Fig. 1a, we leverage the state-of-the-art standard CMOS patterning technology on 300 mm wafers by fabricating ultra-dense periodic arrays of silicon nanopillars (Fig. 1b and c). By deep ultraviolet (DUV) immersion lithography with sequential double line exposures using a mask of 45 nm width and 45 nm spacing, a pitch down to 90 nm has been accomplished. The plasmonic hot spots are subsequently obtained by coating the nanopatterned silicon substrate with a thin Au film, and by carefully controlling the thickness of the Au film, sub-10 nm gaps are achieved (Fig. 1d and e). To the best of our knowledge, SERS substrates with such a high regular array

[a]*IMEC, Kapeldreef 75, B-3001 Leuven, Belgium. E-mail: lijackie@imec.be, chang.chen@imec.be*
[b]*INPAC and Department of Physics and Astronomy, KU Leuven, Celestijnenlaan 200 D, B-3001 Leuven, Belgium*
[c]*Panasonic Corporation, 3-4 Hikaridai, Seika-cho, Soraku-gun, Kyoto 619-0237, Japan*

†Electronic supplementary information (ESI) available: SEM images of nanopillar substrates, FDTD simulation details, electric field enhancement maximum on the Au nanospheroid surface, substrate SERS enhancement factor calculation, batch-to-batch reproducibility. See DOI: 10.1039/c4nr04315d

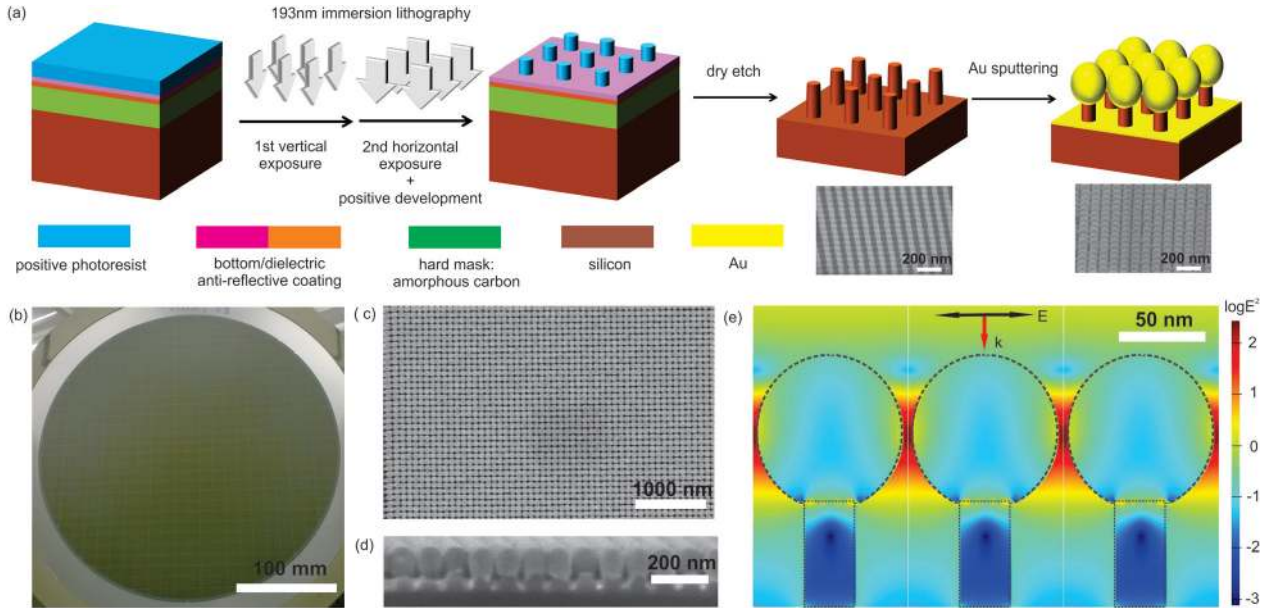

Fig. 1 (a) Schematic of the fabrication of Au-capped nanopillar substrates by DUV immersion lithography and Au sputtering. Two SEM images are shown below the corresponding nanostructures. (b) An optical image of the 300 mm wafer Si nanopillar substrate. SEM images of the ultra-dense nanopillar array with 80 nm Au sputtering on 70 nm height Si nanopillars viewed from (c) top, and (d) side cross-section. (e) The corresponding FDTD simulated profile of the electric field enhancement distribution at the 785 nm light excitation. The black dashed lines are the outline of the Au capped Si nanopillars. The black and red arrows indicate the polarization and incidence direction of the excitation light, respectively.

density and small gap size have not been reported before. Our substrates highlight not only a superior SERS signal reproducibility, but also easy accessibility to the target analyte and good robustness. We further evaluate the SERS performance under both 785 nm and 633 nm laser illuminations, and a simplified finite difference time domain (FDTD) model is adopted to interpret the correlation between the SERS intensity and the Au deposition thickness.

Results and discussion

The properties of the nanopillars could be fine-tuned by adjusting the Si etch time and the Au deposition thickness. We investigated relatively short pillars with heights H_{pillar} = 70 nm and 150 nm to ensure good robustness for the successive fabrication steps and measurements. Detailed fabrication and characterization methods are available in Section 1 of the ESI.† It is generally accepted that the SERS enhancement is optimal between nanogaps. Therefore, on the Si nanopillars with a diameter of 30 nm, we sputtered a series of Au with thicknesses ranging from 30 nm to 100 nm in order to optimize the SERS signals. In contrast to the evaporation method, the sputtering deposition adopted here ensures the 3D growth of the Au caps on top of the nanopillars, shrinking the interpillar separations as the Au deposition thickness increases. As the Au cap size grows, the gap size between them becomes smaller and sub-10 nm gaps are obtained when an Au thickness of 80 nm is deposited as shown in Fig. 1d. It is also observed that a few gaps are closed and the Au caps start to touch each other, forming connecting Au islands (Fig. 1c). The start of this touching effect is in fact beneficial to the field enhancement as will be discussed in the following. Nevertheless, beyond this critical thickness, though narrow gaps are also observed, more touching between the Au caps is present as shown in Fig. S1 in the ESI.†

When metal nanostructures are placed in close adjacency, the plasmon resonances strongly interact and their overall response can be very different from that of the individual nanostructures.[26] The substrates we fabricated contain in fact a very high density of interacting Au nanocaps, where their global optical response is expected to smear out spectrally similar to aggregates of metal nanoparticles. Indeed, as shown in the reflection spectra measured with a Bruker Vertex 80v Fourier transform infrared spectrometer (Fig. 2a and c), no sharp plasmonic resonances are observed for both nanopillar heights under investigation. In substrates with a thicker Au layer, nearly all the incident light is reflected in the near infrared. To gain more insight into the local optical response of the Au-capped Si nanopillar arrays, we executed numerical FDTD simulations using Lumerical FDTD Solutions. Specifically, we implemented a FDTD model of Au nanospheroids standing on top of cylindrical Si nanopillars on a semi-infinite Si. The simulated reflection spectra are presented in Fig. 2b and d, and they fit the experimental measurements well. Refer to Section 3 of the ESI† for more FDTD details.

In spite of the fact that no sharp and pronounced plasmonic resonances are observed, this ultra-dense 'hot spot' array is promising for broadband SERS applications in the visible and near infrared range. Using 4-aminothiophenol (4-ATP) as a

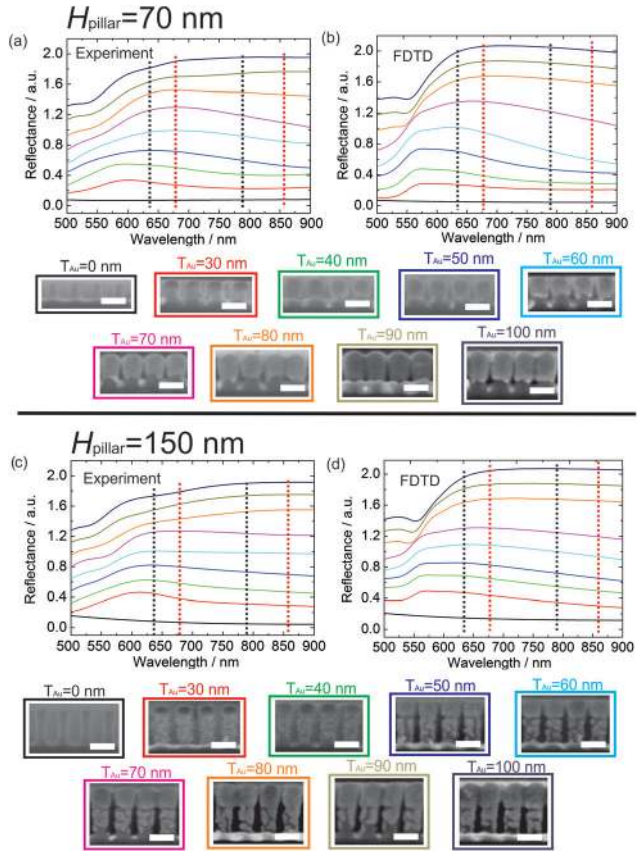

Fig. 2 (a, c) Experimental and (b, d) FDTD simulated reflection spectra for the Au-capped nanopillar arrays with the nanopillar heights of 70 nm and 150 nm. A series of Au thicknesses from 30 nm to 100 nm are deposited on the Si nanopillar arrays, and the corresponding cross section SEM images are exhibited at the bottom. The scale bars in the SEM images represent 100 nm. The spectra are offset for clarity. The black dashed lines indicate the excitation wavelengths used in SERS measurements (633 nm and 785 nm), and the red ones are the corresponding Stokes shifted wavelengths for the 4-ATP 1078 cm^{-1} vibrational mode (679 nm and 857 nm).

probe molecule, the SERS spectra for the H_{pillar} = 70 nm and H_{pillar} = 150 nm substrates were investigated at both 785 nm and 633 nm laser excitations, and the results are presented in Fig. 3. Typically, the intensity of the C–S bond stretching vibrational mode at ~1078 cm^{-1}, which is highlighted in the green dashed box, increases from T_{Au} = 30 nm to T_{Au} = 80 nm Au depositions, as with the increasing Au thickness, the inter-pillar gaps narrow. For thicker Au layers, the intensity drops as a consequence of the touching Au caps. The T_{Au} = 80 nm substrates, for which we have achieved the smallest gap size and lowest touching degree, show the maximum SERS intensities. Comparisons between the H_{pillar} = 70 nm and H_{pillar} = 150 nm substrates also indicate that the former produce higher SERS signals.

The detected SERS signal is a complicated puzzle that deserves thorough scrutiny.[27,28] Typically it originates from EM and chemical enhancement mechanisms. The EM mechanism states that the enhancement factor (EF) equals the electric field intensity enhancement at the incidence wavelength multiplied by the enhancement at the Stokes shifted wavelength,

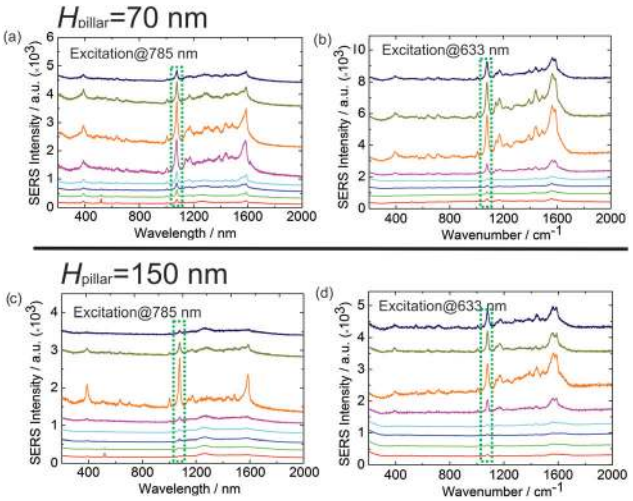

Fig. 3 4-ATP SERS spectra measured at (a, c) 785 nm and (b, d) 633 nm wavelength excitations for the Au-capped nanopillar arrays with the nanopillar heights of 70 nm and 150 nm. The Au layer thicknesses range from 30 nm to 100 nm (same colour corresponding to the Au thickness as in Fig. 2). The spectra are offset for clarity. The green dashed box indicates the 4-ATP C–S bond stretching vibrational mode at ~1078 cm^{-1}.

which could be approximated as the E^4 rule ($E^4 = E^2_{incidence} \times E^2_{Stokes}$). It is also established that the hot spots contribute more to the total SERS enhancement.[29,30] In our substrates, the maximum E^2 enhancement on the Au nanospheroid surface is also simulated as a function of the incidence wavelength (ESI, Fig. S2†), which confirms that at the incidence and Stokes wavelengths no pronounced resonances arise. This implies that the SERS signal mainly results from the non-resonant enhancement of the electric field intensity in the regions between the Au nanocaps. As displayed in Fig. 1c, since both the nanogaps, where the Au caps do not touch and the touching of the Au nanocaps are present in the array, the SERS enhancement is categorized into two effects as illustrated in Fig. 4.

For the thinner Au deposition (T_{Au} < 70 nm), the SERS signal enhancement is dominated by the high electric field enhancement located in the gap regions. Nanogaps are also observed in arrays with thicker Au coatings as shown in Fig. S1.† We call the field enhancement in these non-touching regions the "non-touching" effect. The enhancement factors due to the non-touching effect strongly depend not only on the minimum distance between the gold surfaces of adjacent nanospheroids (gap size), but also on other geometrical parameters such as the vertical nanospheroid diameter and the nanopillar height. While usually only the maximum field enhancement is considered in the EF calculation, here in order to take into account the overall topography of the electric intensity profile we will integrate the calculated $E^2_{incidence} \times E^2_{Stokes}$ product over the nanospheroid surface. As presented in Fig. 4a and b, at both excitation wavelengths and for both nanopillar heights, this integrated field enhancement generally fits the trend of the experimental SERS signals. The spatially integrated field enhancement is a better fit to the experimental results in the sense that it considers the whole

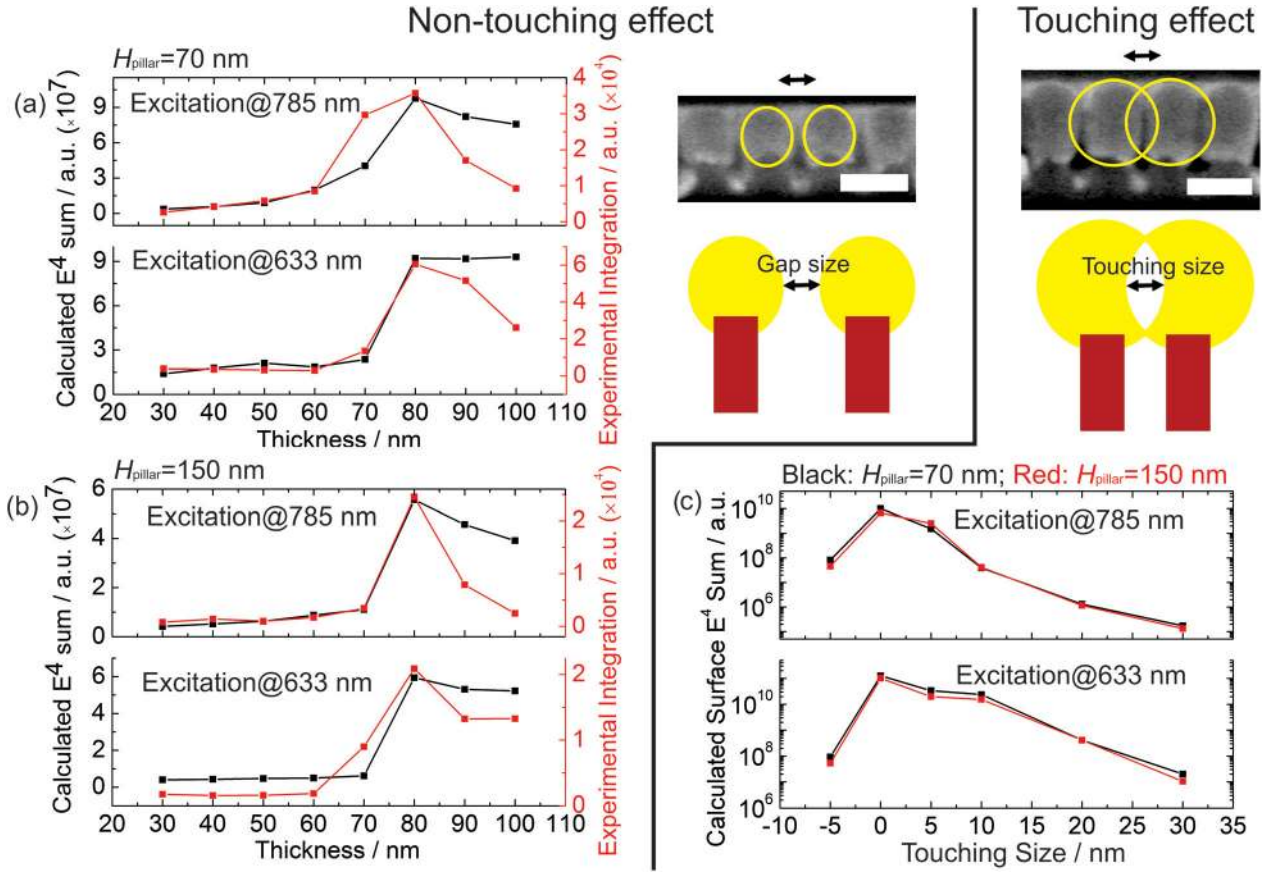

Fig. 4 SERS signal enhancement interpretations based on FDTD simulations: (a, b) non-touching effect and (c) touching effect. For the Au caps that do not touch (*e.g.* prevalent in arrays with Au coating thicknesses of less than 70 nm, and also present in arrays with thicker Au coatings), the electric field intensity enhancement at the nanogap regions dominates. Here the non-touching effect applies. The calculated E^4 sum across the nanospheroid surface, the black curves corresponding to the left axes, and the experimentally integrated SERS intensities, the red curves to the right axes, are demonstrated as a function of the Au deposition thickness for the nanopillar heights of (a) 70 nm and (b) 150 nm, respectively. For arrays with thicker Au depositions, in addition to the non-touching effect, some of the Au caps start to touch and decrease the SERS intensity. (c) The calculated E^4 sum across the Au nanospheroid surface as a function of the touching size for the Au deposition thickness of 90 nm while keeping the vertical nanospheroid diameter as a constant. The touching size is defined as the diameter of the imaginary nanospheroid in the in-plane dimension minus the distance between adjacent nanospheroid centers as shown in the schematic of Fig. 3c. Yellow spheroids in the SEM images approximate the outline of the Au caps.

landscape of the electric field enhancement distribution across the nanospheroid surface instead of only the maximum E^4 enhancement at a specific position. In addition, the FDTD analysis shows that the surface E^4 sum for the H_{pillar} = 70 nm substrates is larger than that for H_{pillar} = 150 nm substrates. This could be attributed to the fact that the short nanopillars support a stronger constructive interference of the reflected light in the nanogap regions. Moreover, the higher Si nanopillars could absorb more light and effectively damp the plasmon, also reducing the SERS signals.

Moreover, it is noted that for the arrays with thicker Au depositions ($T_{Au} \geq 90$ nm), the experimental SERS signal intensity is smaller than the integrated E^4 enhancement predicted by the non-touching effect. This is because for these thicker Au coatings, in addition to the non-touching effect, the "touching" effect of the Au caps will eventually decrease the SERS signal. As more Au is deposited, a small fraction of the Au caps start to touch. Conceptually, at the beginning of the touching more enhanced hot spots will appear, resulting in further amplified signals (*e.g.* for arrays with gap sizes close to zero). As the deposition continues, larger fractions of the Au caps are touching and more nanogaps start to diminish, impairing the SERS enhancement. As the FDTD simulation results demonstrate in Fig. 4c, the calculated surface E^4 sum for the T_{Au} = 90 nm substrates increases for a small touching size, and decreases when the touching size grows. This idea also corroborates the fact that it is the T_{Au} = 80 nm arrays, in which clear touching just starts to show up, that presents the highest SERS signals. For these arrays with thicker Au coatings, the actual SERS signal enhancement could be considered as a combination of both the non-touching and touching effects. As a thicker Au layer is deposited, the fraction of touching nanocaps increases, resulting in reduced SERS signals. Therefore, fine-tuned Au deposition is critical to achieve optimized SERS signals.

In the H_{pillar} = 150 nm substrates, it is clear from the SEM images in Fig. 2 that on the Si nanopillar sidewalls there are

Au nanoislands caused from the sputtering deposition. As previously reported,[14,15] these nanoislands could form gap-rich nanostructures that also contribute to the SERS signal enhancement. Nevertheless, in our highly dense arrays the SERS enhancement results from the gaps between the top Au caps instead. The simplified FDTD model without such sidewall nanoislands has already demonstrated an adequately good fit to the detected SERS intensities. In addition, the H_{pillar} = 70 nm substrates, which lack the sidewall Au nanoislands, show an even higher SERS signal.

A limiting factor in the further widespread applications of the SERS technique is the trade-off between the high signal amplification and good uniformity. Nevertheless, since the major advantage of our Si nanopillar array is its high uniformity on a wafer scale, the Au capped substrates are expected to show a high SERS signal reproducibility. We compared our Au-capped nanopillar SERS substrates to the commercial Klarite™ from Renishaw Diagnostics. Among the best ever reported, Klarite™ SERS substrates are tested to show a relative signal standard deviation of better than 10%.[11,12] In addition, the geometry of the Klarite™ substrates, which are inverted Si pyramid arrays covered with Au, has been optimized for the coupling of localized and propagating surface plasmon modes to give resonances at 633 nm and 785 nm.[12] The Klarite™ hot spots are localized at the bottom and the top corners of the inverted pyramids with a pitch of ~2 μm. Since the uniformity of SERS signal largely depends on the experimental conditions, especially the laser spot size, it is recommended to use a >5 μm spot for the SERS excitation to ensure that adequate amounts of inverted pyramids are illuminated. In our SERS measurement, a 10× water immersion objective with a laser spot of ~5 μm was used to fulfill the Klarite™ recommendation, and the SERS intensities are measured over a distance of 200 μm in a step of 1 μm. The mean intensity and standard deviation are calculated by integrating the 1078 cm^{-1} Raman band, and the coefficient of variation (CV) is defined as the standard deviation divided by the mean intensity, which is an indication of the SERS substrate uniformity. The comparison results between the Klarite™ and our nanopillar substrates (T_{Au} = 80 nm) are shown in Fig. 5. It demonstrates that the Au-capped nanopillar arrays not only present a higher SERS signal, but also a lower fluctuation/CV level. On the one hand, the improved signal reproducibility is related to the state-of-the-art nanofabrication process, which offers the high degree of inherent uniformity with an array pitch of less than 100 nm. On the other hand, it is attributed to the large number of hot spots that are easily accessible to the target analytes within the laser spot (~2.5×10^3 unit structures for our nanopillar substrates, compared to only ~5 for Klarite™, although the Au surface areas are similar). Compared to the literature with improved signal reproducibility,[9,10] our nanopillar substrates benefit from the large wafer level fabrication method. In addition, it features the sub-10 nm gap size which gives rise to the largely enhanced SERS signals.[16]

The substrate SERS EFs of our Au capped nanopillar arrays have also been experimentally calculated as shown in Section 5 of the ESI.† It is noted that the EF calculation depends on the molecular coverage assumption adopted, and a variation as large as ~10^5 can be obtained.[19] Under the full monolayer coverage assumption, an average EF on the order of ~10^5 is attained in our calculation, while if the few molecule coverage assumption is taken,[31] the EF can be ~10^9. In addition, since the nanogaps, the non-touching regions of the Au caps, and the touching of the caps are both present in the T_{Au} = 80 nm substrates, these experimental substrate EFs are the average values by taking into account both effects. The EF at particular Au cap positions with narrower gaps could be higher. In Table S2 in the ESI,† the simulated $E^4 = E^2_{incidence} \times E^2_{Stokes}$ at the maximum field enhancement positions on the surface for both non-touching and touching effects are also listed, which range from ~10^4 to ~10^8 depending on the gap sizes and excitation wavelengths. Therefore, the EF of our substrates could be sufficiently large for single molecule SERS detection, especially considering the high hot spot density and easy molecule accessibility.[32–35]

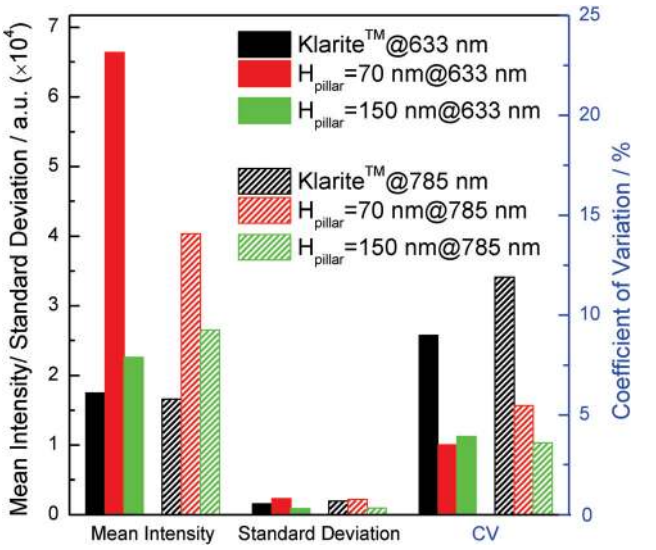

Fig. 5 Uniformity comparisons of the T_{Au} = 80 nm substrates with the commercial Klarite™. Compared to the Klarite™ substrate (CV ~ 10%), the uniformity of the nanopillar supported substrates is much improved (CV ~ 4%).

The goal of our current work is not to demonstrate an extremely large EF, but to present a scalable method to produce reliable SERS substrates with improved uniform and reproducible signals. The results in Fig. 5 show that under the same experimental conditions, our nanopillar substrates surpass the commercial Klarite™ substrates with an improved SERS performance. Batch-to-batch reproducibility of our SERS substrates has also been investigated, and they demonstrate good reliability as well (Section 6 in the ESI†).

Conclusions

In conclusion, we have introduced a method to realize large wafer scale preparation of exceptionally dense arrays of plas-

monic hot spots with sub-10 nm gaps, and have demonstrated that these substrates support both high SERS enhancement factors and excellent uniformity and reproducibility. Specifically, employing the state-of-the-art CMOS front-end patterning techniques allowed us to develop a 300 mm wafer scale process for the fabrication of ultra-dense arrays of Si nanopillars, which we subsequently coated with Au films to obtain a pattern of Au nanocaps with sub-10 nm gaps. We have investigated the SERS performance of substrates under both 785 nm and 633 nm excitations. Largely enhanced and uniform SERS signals have been obtained in the ultra-dense arrays and compared to the commercial Klarite™ substrates. Though no pronounced plasmonic resonances are detected, FDTD simulations illustrate that the amplified SERS signals are mainly derived from the electric field enhancement in the regions between the Au caps. Due to the large signal enhancement, high uniformity and wafer scale fabrication capacity, the Au-capped nanopillar substrates are promising for the detection of small molecules in label-free biosensing applications.

Acknowledgements

C.C. and N.V. gratefully acknowledge the financial support from FWO (Flanders). N.V. and V.V.M. are supported by the Methusalem funding by the Flemish Government.

Notes and references

1 A. Polemi, S. M. Wells, N. V. Lavrik, M. J. Sepaniak and K. L. Shuford, *J. Phys. Chem. C*, 2011, **115**, 13624–13629.
2 J. D. Caldwell, O. Glembocki, F. J. Bezares, N. D. Bassim, R. W. Rendell, M. Feygelson, M. Ukaegbu, R. Kasica, L. Shirey, C. Hosten and C. E. T. Al, *ACS*, 2011, **5**, 4046–4055.
3 G. H. Gu, J. Kim, L. Kim and J. S. Suh, *J. Phys. Chem. C*, 2007, **111**, 7906–7909.
4 C. Chen, J. A. Hutchison, P. Van Dorpe, R. Kox, I. De Vlaminck, H. Uji-I, J. Hofkens, L. Lagae, G. Maes and G. Borghs, *Small*, 2009, **5**, 2876–2882.
5 Z. Huang, G. Meng, Q. Huang, Y. Yang, C. Zhu and C. Tang, *Adv. Mater.*, 2010, **22**, 4136–4139.
6 D.-K. Lim, K.-S. Jeon, H. M. Kim, J.-M. Nam and Y. D. Suh, *Nat. Mater.*, 2010, **9**, 60–67.
7 L. a. Dick, A. D. McFarland, C. L. Haynes and R. P. Van Duyne, *J. Phys. Chem. B*, 2002, **106**, 853–860.
8 S. Gómez-Graña, J. Pérez-Juste, R. a. Alvarez-Puebla, A. Guerrero-Martínez and L. M. Liz-Marzán, *Adv. Opt. Mater.*, 2013, **1**, 477–481.
9 W. J. Cho, Y. Kim and J. K. Kim, *ACS Nano*, 2012, **6**, 249–255.
10 N. G. Greeneltch, M. G. Blaber, A.-I. Henry, G. C. Schatz and R. P. Van Duyne, *Anal. Chem.*, 2013, **85**, 2297–2303.
11 M. E. Hankus, D. N. Stratis-cullum and P. M. Pellegrino, in *SPIE-Optics and Photonics West*, 2011, vol. 8099, pp. 8099–8107.
12 N. M. B. Perney, J. J. Baumberg, M. E. Zoorob, M. D. B. Charlton, S. Mahnkopf and C. M. Netti, *Opt. Express*, 2006, **14**, 847–857.
13 K. Malachowski, R. Verbeeck, T. Dupont, C. Chen, Y. Li, S. Musa, T. Stakenborg, D. Sabuncuoglu Tezcan and P. Van Dorpe, *ECS Trans.*, 2013, **50**, 413–422.
14 W. Li, F. Ding, J. Hu and S. Y. Chou, *Opt. Express*, 2011, **19**, 3925–3936.
15 Y.-J. Oh and K.-H. Jeong, *Adv. Mater.*, 2012, **24**, 2234–2237.
16 U. S. Dinish, F. C. Yaw, A. Agarwal and M. Olivo, *Biosens. Bioelectron.*, 2011, **26**, 1987–1992.
17 J. D. Caldwell, O. J. Glembocki, F. J. Bezares, M. I. Kariniemi, J. T. Niinistö, T. T. Hatanpää, R. W. Rendell, M. Ukaegbu, M. K. Ritala, S. M. Prokes, C. M. Hosten, M. a. Leskelä and R. Kasica, *Opt. Express*, 2011, **19**, 26056–26064.
18 A. Shevchenko, V. Ovchinnikov and A. Shevchenko, *Appl. Phys. Lett.*, 2012, **100**, 171913.
19 M. S. Schmidt, J. Hübner and A. Boisen, *Adv. Mater.*, 2012, **24**, OP11–OP18.
20 X. Yang, H. Zhong, Y. Zhu, J. Shen and C. Li, *Dalton Trans.*, 2013, **42**, 14324–14330.
21 R. Lu, J. Sha, W. Xia, Y. Fang, L. Gu and Y. Wang, *CrystEngComm*, 2013, **15**, 6207.
22 F. Ou, M. Hu, I. Naumov and A. Kim, *Nano Lett.*, 2011, **11**, 2538–2542.
23 M. A. Rafiq, H. Mizuta, S. Uno and Z. A. K. Durrani, *Microelectron. Eng.*, 2007, **84**, 1515–1518.
24 H. C. Jeon, C.-J. Heo, S. Y. Lee and S.-M. Yang, *Adv. Funct. Mater.*, 2012, **22**, 4268–4274.
25 X. Yang, N. Ileri, C. C. Larson, T. C. Carlson, J. A. Britten, A. S. P. Chang, C. Gu and T. C. Bond, *Opt. Express*, 2012, **20**, 24819–24826.
26 P. K. Jain, W. Huang and M. a. El-Sayed, *Nano Lett.*, 2007, **7**, 2080–2088.
27 S. M. Morton, D. W. Silverstein and L. Jensen, *Chem. Rev.*, 2011, **111**, 3962–3994.
28 E. C. Le Ru, M. Meyer and P. G. Etchegoin, *J. Phys. Chem. B*, 2006, **110**, 1944–1948.
29 C. Chen, J. A. Hutchison, F. Clemente, R. Kox, H. Uji-I, J. Hofkens, L. Lagae, G. Maes, G. Borghs and P. Van Dorpe, *Angew. Chem., Int. Ed.*, 2009, **48**, 9932–9935.
30 Y. Fang, N.-H. Seong and D. D. Dlott, *Science*, 2008, **321**, 388–392.
31 M. Hu, F. S. Ou, W. Wu, I. Naumov, X. Li, A. M. Bratkovsky, R. S. Williams and Z. Li, *J. Am. Chem. Soc.*, 2010, **132**, 12820–12822.
32 E. C. Le Ru, E. Blackie, M. Meyer and P. G. Etchegoin, *J. Phys. Chem. C*, 2007, **111**, 13794–13803.
33 P. G. Etchegoin and E. C. Le Ru, *Phys. Chem. Chem. Phys.*, 2008, **10**, 6079–6089.
34 J. P. Camden, J. a. Dieringer, Y. Wang, D. J. Masiello, L. D. Marks, G. C. Schatz and R. P. Van Duyne, *J. Am. Chem. Soc.*, 2008, **130**, 12616–12617.
35 D. Wang, W. Zhu, M. D. Best, J. P. Camden and K. B. Crozier, *Sci. Rep.*, 2013, **3**, 2867.

